Electronic Supplementary Material (ESI) for Journal of Materials Chemistry A.

Supporting Information

Tunable mesoporous manganese oxide for high performance oxygen reduction and evolution reactions

Islam M. Mosa[1,2†], Sourav Biswas[1†], Abdelhamid M. El-Sawy[1,2], Venkatesh Botu[4], Curtis Guild[1], Wenqiao Song[1], Rampi Ramprasad[4], James F. Rusling[1,3,5], Steven L. Suib[1, 6*]

[1]Department of Chemistry, University of Connecticut, 55 North Eagleville Road, Storrs, Connecticut 06269, United States
[2]Department of Chemistry, Tanta University, Tanta 31527, Egypt
[3]Department of Cell Biology, University of Connecticut Health Center, Farmington, Connecticut 06032, United States
[4]University of Connecticut, Chemical and Biomolecular Engineering, 97 North Eagleville Road, Unit 3136, Storrs, Connecticut 06269, United States

[5]School of Chemistry, National University of Ireland, Galway, University Road, Galway, Ireland

[6]Institute of Materials Science, University of Connecticut, U-3060, 55 North Eagleville Rd., Storrs, Connecticut 06269, United States

[†] I.M and S.B contributed equally

Chemicals

Manganese (II) nitrate tetrahydrate ($Mn(NO_3)_2.4H_2O$, ≥ 97.0) cesium nitrate ($CsNO_3$, ≥ 99.0), 1-butanol (anhydrous, 99.8%), and Poly (ethylene glycol)- block- Poly(propylene glycol)-block-Poly(ethylene glycol) PEO_{20}-PPO_{70}-PEO_{20} (Pluronic P123), concentrated nitric acid (HNO_3, 68-70 %), manganese (III,IV,II) oxides (≥ 99.99), iridium chloride hydrate ($IrCl_3.xH_2O$), platinum on graphitized carbon 20% by weight, ruthenium(IV) oxide (RuO_2, 99.9 %), Nafion 117 solution (5 % in alcohol-water mixture), and potassium hydroxide (KOH, ≥ 85 %) were purchased from Sigma-Aldrich. All chemicals were used as received without further purification.

Catalyst Characterization

The powder X-Ray diffraction (PXRD) measurements were performed on a Rigaku Ultima IV diffractometer (Cu Kα radiation, λ=1.5406 Å) with an operating voltage of 40 kV and a current of 44 mA. The PXRD patterns were collected over a 2θ range of 5–75° with a continuous scan rate of 1.0° min^{-1}. The nitrogen adsorption desorption experiments were performed with a Quantachrome Autosorb-1-1C automated adsorption system. The samples were degassed at 150°C for 6 h under helium prior to measurement. The surface areas were calculated using the Brunauer–Emmett–Teller (BET) method and the Barrett–Joyner–Halenda (BJH) method was used to calculate the pore sizes and pore volumes from the desorption branch of the isotherm. The surface morphology was determined by a Zeiss DSM 982 Gemini field emission scanning electron microscope (FE-SEM) with a Schottky emitter at an accelerating voltage of 2.0 kV having a beam current of 1.0 mA. High-resolution transmission electron microscopy (HR-TEM) experiments were carried out on a JEOL 2010 FasTEM microscope with an operating voltage of 200 kV. The samples were prepared by casting the suspension of material on a carbon coated copper grid. Tapping mode AFM was performed by loading the catalyst on a bare mica disc. Temperature-resolved *in situ* powder X-ray diffraction (TR-PXRD) analysis was done in an XTRA X-ray diffractometer (Cu Kα radiation) equipped with an Anton Parr XRK 900 heating chamber. The structural changes of the Cs-promoted MnOx and the non-promoted MnOx materials were investigated from 250°C to 650°C using a ramp rate of 5°C min^{-1} under air. Diffraction patterns were obtained in the range of 5-75° 2θ at a scanning rate of 2.0° min^{-1}. X-ray photoelectron spectroscopy (XPS) was done on a PHI model

590 spectrometer with multiprobes (ΦPhysical Electronics Industries Inc.), using Al-K radiation (λ= 1486.6 eV) as the radiation source and fitted using CasaXPS software (version 2.3.12). The powder samples were pressed on carbon tape mounted on adhesive copper tape stuck to a sample stage placed in the analysis chamber. For correction of surface charging, the C 1s photoelectron line at 284.6 eV was taken as a reference. A mixture of Gaussian (70%) and Lorentzian (30%) functions was used for the least-squares curve fitting procedure. The X-ray absorption near-edge spectra (XANES) and extended X-ray absorption fine structure (EXAFS) were measured at the National Synchrotron Light Source (NSLS) at Brookhaven National Lab using beamline X18A. The synchrotron radiation energy was monochromatize using a Silicon (111) channel-cut double crystal monochromator. The incident and transmitted beam intensities were monitored using ionization chambers filled with a mixture of nitrogen and helium. The samples diluted by h-BN with a ratio of (1:8) were then pressed into pellets. The XANES data were analyzed with Athena software where background, post, and pre-edge corrections were made. The CO_2 chemisorption experiments were performed using a Quantachrome Autosorb-1-1C automated adsorption system. All the samples were heated in helium under vacuum at 150°C for 6 h prior to experiments. The adsorption studies were done at room temperature, 0°C, and -78°C.

Conversion of standard calomel electrode (SCE) to relative hydrogen electrode (RHE)

Since all electrochemical experiments were performed in 0.1 M KOH (pH = 13):

E^0 = 1.230 V - 0.0591 (pH)

E^0 = 1.230 V - 0.0591 (13)

Therefore, E^0 = 0.463 vs. RHE

Since the potential difference between SCE and RHE is 0.244 V, so

E^0 = 0.463 - 0.244 = 0.219 vs. SCE

Overpotential (η) = Potential vs. SCE - 0.219 V

E vs. RHE = E vs. SCE + (1.23 - 0.219) = E vs. SCE + 1.01 V

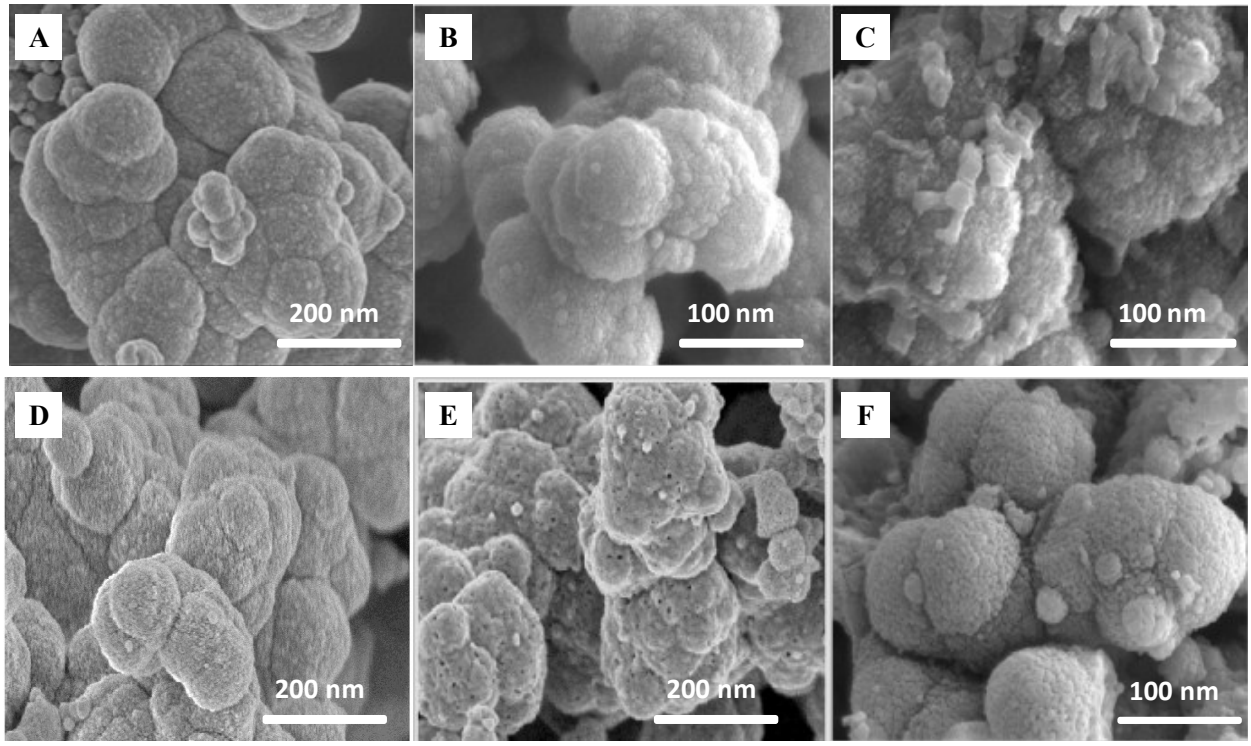

Fig. S1 FE-SEM images of Cs-MnOx materials calcined at (A) 250 °C, (B) 350 °C, (C) 400 °C, (D) 450 °C, (E) 550 °C and (F) 650 °C.

Table S1: Structural parameters of Cs promoted mesoporous manganese oxide samples

Sample ID	Heat treatment[a]	Surface area (m^2/g)[b]	Pore size (nm)[c]	Pore volume (cc/g)[c]
Cs-MnOx-250	250 °C for 3 h	79	3.4	0.10
Cs-MnOx-350	350 °C for 2 h	106	3.4	0.18
Cs-MnOx-450	450 °C for 2 h	86	4.9	0.18
Cs-MnOx-550	550 °C for 1 h	53	7.8	0.17
Cs-MnOx-650	650 °C for 1 h	13	NA	0.11

[a]Consecutive heat treatment. [b]Determined by BET method. [c]Calculated by BJH method from the desorption branch of the isotherms, NA stands for not applicable. All materials were heated at 150 °C for 12 h prior to the heating cycles.

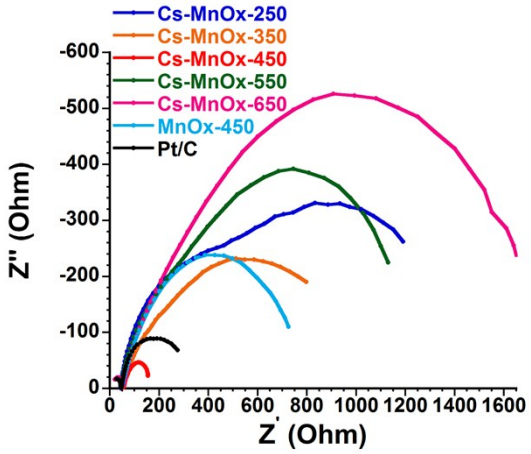

Fig. S2 Nyquist plots obtained from the electrochemical impedance spectroscopy measurements at an anodic polarization potential of - 0.15 V vs. SCE (0.86 vs. RHE).

Table S2. The exchange current density obtained from charge transfer resistance of the different studied catalysts towards ORR and OER. The EIS was measured at -0.15 V vs. SCE (0.86 V vs. RHE) for ORR, and 0.7 V vs. SCE (1.71 V vs. RHE) for OER.

Catalyst	ORR J_o (A cm^{-2})	OER J_o (A cm^{-2})
Cs-MnOx-250	4.6E-05	9.44E-02
Cs-MnOx-350	7.1E-05	1.52E-01
Cs-MnOx-450	3.7E-04	7.78E-01
Cs-MnOx -550	4.5E-05	1.08E-01
Cs-MnOx-650	2.5E-05	2.68E-02
MnOx-450	7.0E-05	2.84E-01
20 % wt. Pt/C	1.9E-04	N/A
20 % wt. Ir/C	N/A	1.05E+00

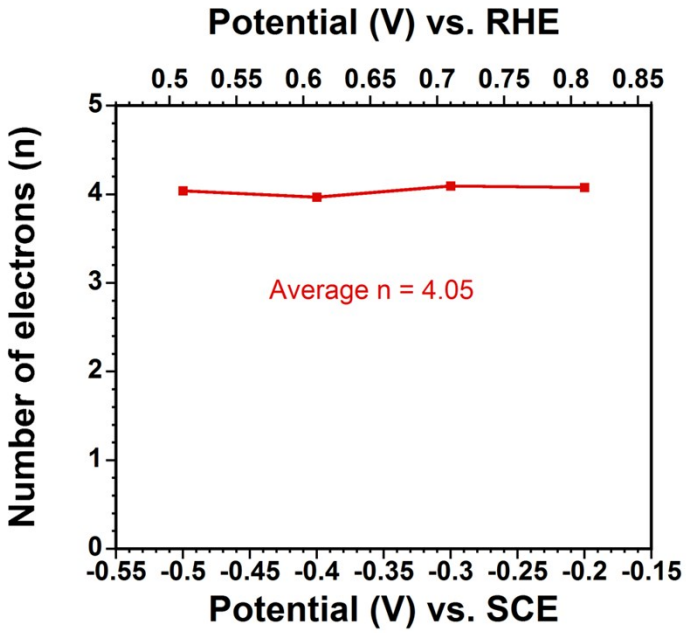

Fig. S3 The change in the number of electron transferred in ORR for the Cs-MnOx-450 at different potentials. The number of electrons was calculated from the slope of the K-L plots.

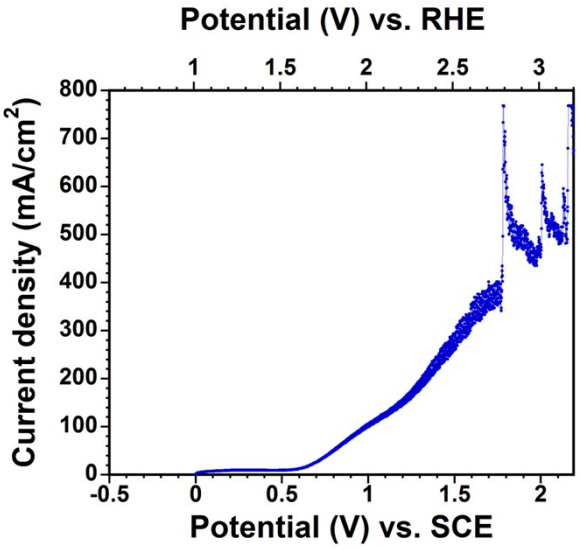

Fig. S4 LSV curve for Cs-MnOx-450 with extended potential window up to 2.2 V vs. SCE at a scan rate of 250 mV/s in 0.1 M KOH, showing ultra-high current.

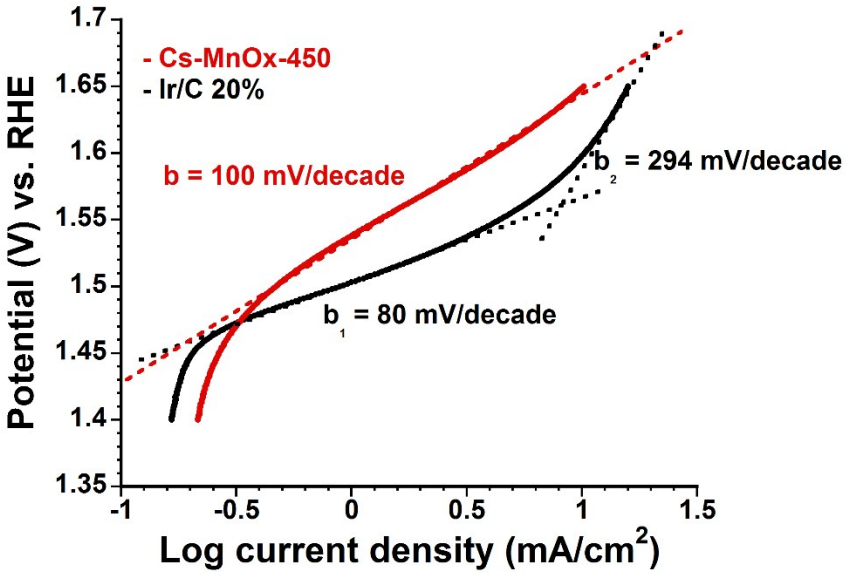

Fig. S5 Tafel plots for the OER of Cs-MnOx-450 as compared to the highly active Ir/C electrocatalyst.

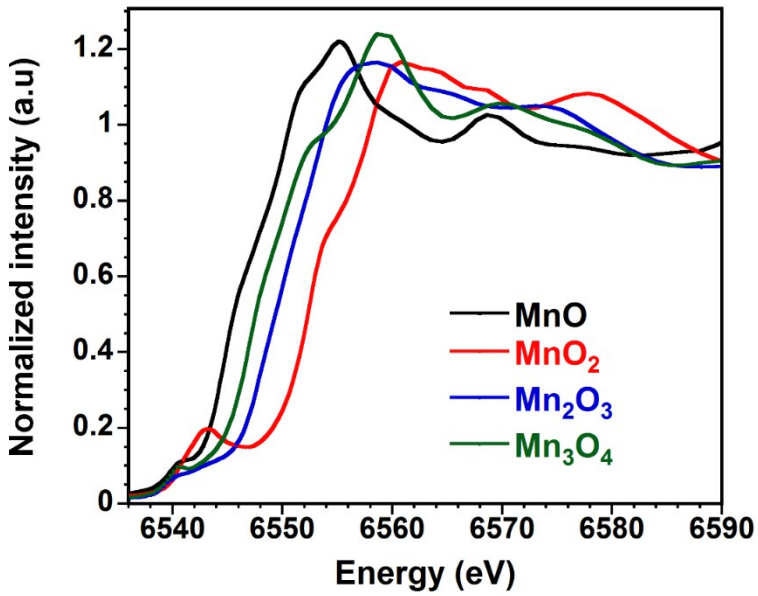

Fig. S6 Mn K edge XANES spectra of the different standard manganese oxides.

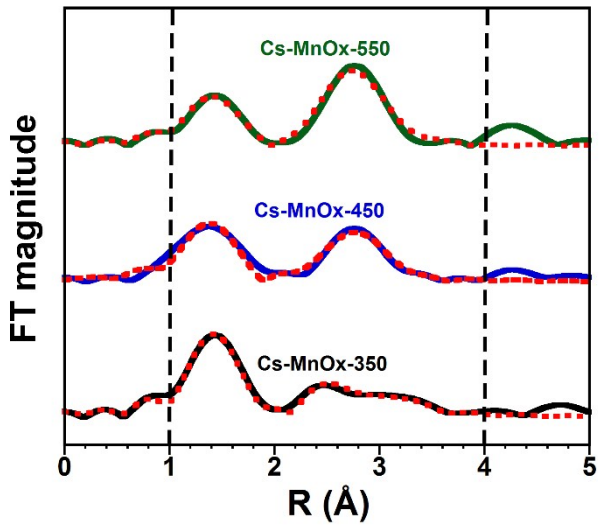

Fig. S7 The k3 weighted Fourier transforms of the Mn K-edge EXAFS spectra for samples calcined at 350 °C to 550 °C. Solid line represent experimental data, and dashed line represent EXAFS theoretical model of bixbyite.

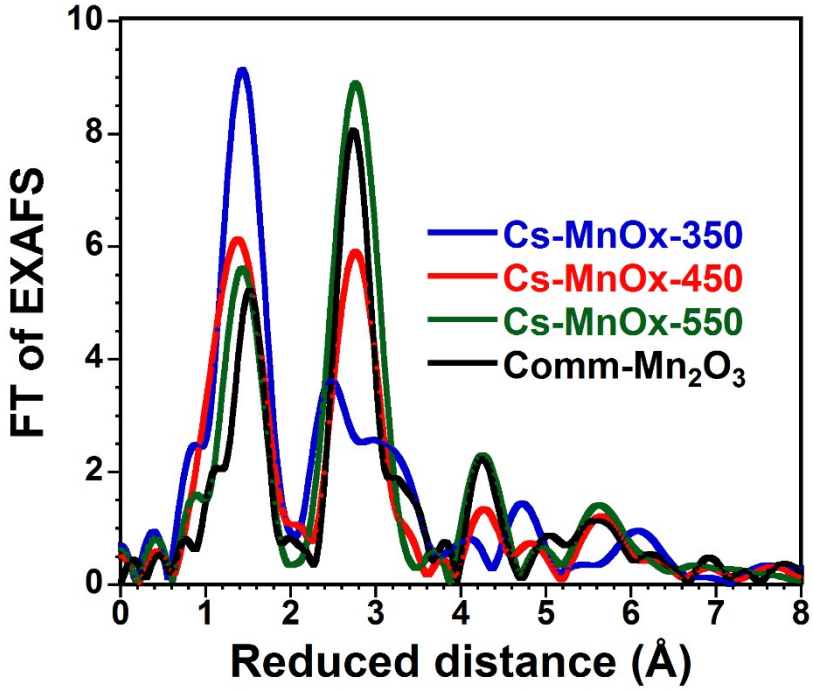

Fig. S8 *Ex situ* EXAFS of Cs-MnOx samples calcined at 350-550 °C compared to commercial non-porous Mn_2O_3.

Table S3: EXAFS fit results. Fit range in *R* space 1.0 Å to 4.0 Å; *k* range from 3 Å to 10 Å; N_{idp} = 20; N_{free} = 9; Bixbyite as theoretical model.

Sample	Path	N	R [Å]	σ^2 [Å^2]	E_0 [eV]
Cs-MnOx-350	Mn-O	3	1.88	0.00208	-1.88
	Mn-Mn	3	2.91	0.01324	
	Mn- Mn	3	3.46	0.00878	
Cs-MnOx-450	Mn-O	3	1.87	0.00525	-6.08
	Mn-Mn	3	3.05	0.01002	
	Mn- Mn	3	3.46	0.01276	
Cs-MnOx-550	Mn-O	3	1.90	0.00736	-4.93
	Mn-Mn	3	3.05	0.00525	
	Mn- Mn	3	3.53	0.00707	

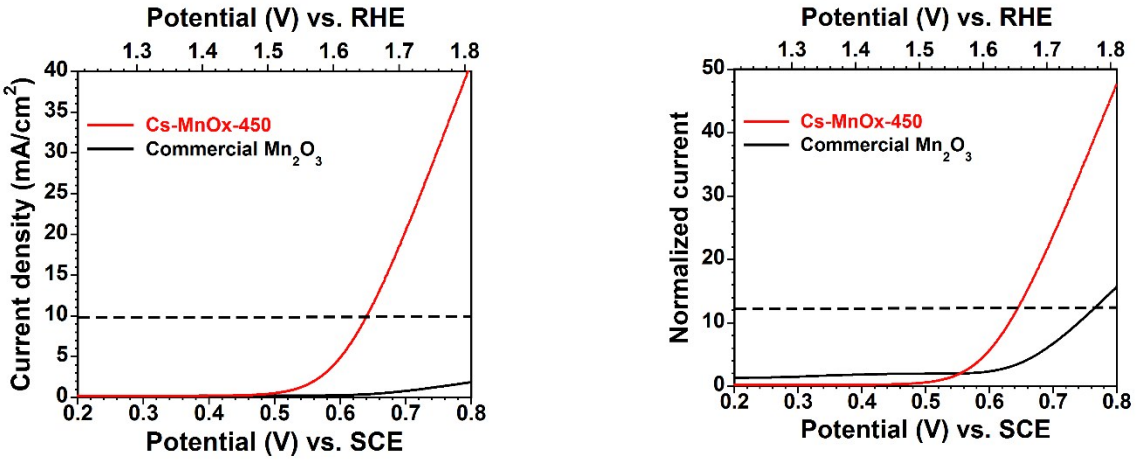

Fig. S9 Comparison of OER activity of Cs-MnOx-450 and commercial Mn_2O_3

Methodology for ECSA determination:

Catalysts were loaded to pyrolytic graphite electrodes as previously described. Cyclic voltammetry was performed at a slow scan rate of 5 mV/s in a potential range of 0.1 - 0.3 V vs, SCE where no faradaic redox reaction occurs. The capacitance was calculated from the rectangular CVs:

$$C_{device} = \frac{\int_{V_1}^{V_n} i(V_2 - V_1)}{\upsilon \quad X \quad \Delta E}$$

where i, V_1, V_2, υ and ΔE are the measured current, the starting voltage, the ending voltage, the scan rate, and the operating potential window.

Table S4: ECSA of Cs-MnOx at different calcination temperatures[a]

Catalyst	Capacitance (mF/cm^2)	Aechem (m^2/g)
Cs-MnOx-250	22	0.13
Cs-MnOx-350	41	0.24
Cs-MnOx-450	20	0.12
Cs-MnOx-550	13	0.08

[a]The electrochemical active surface area can be calculated from the capacitance using an approximation of 60 μF/cm^2 for a full monolayer of catalyst.

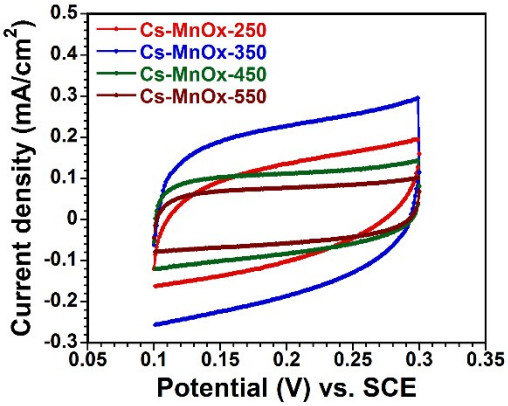

Fig S10 Cyclic voltammograms of the Cs-MnOx materials calcined at different temperatures in 0.1 M KOH at 5 mV/s.

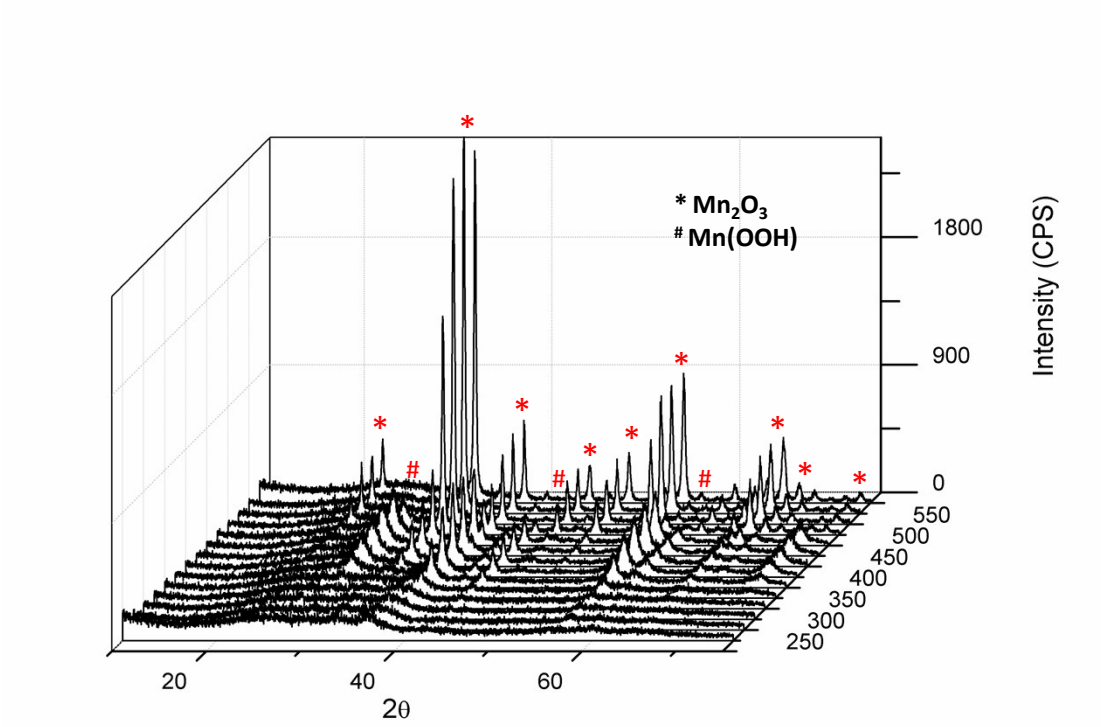

Fig. S11 The temperature resolved powder X-ray diffraction (TR-XRD) MnOx material under air.The material was calcined at 150 °C for 12 h and 250 °C for 3 h prior to measurement.

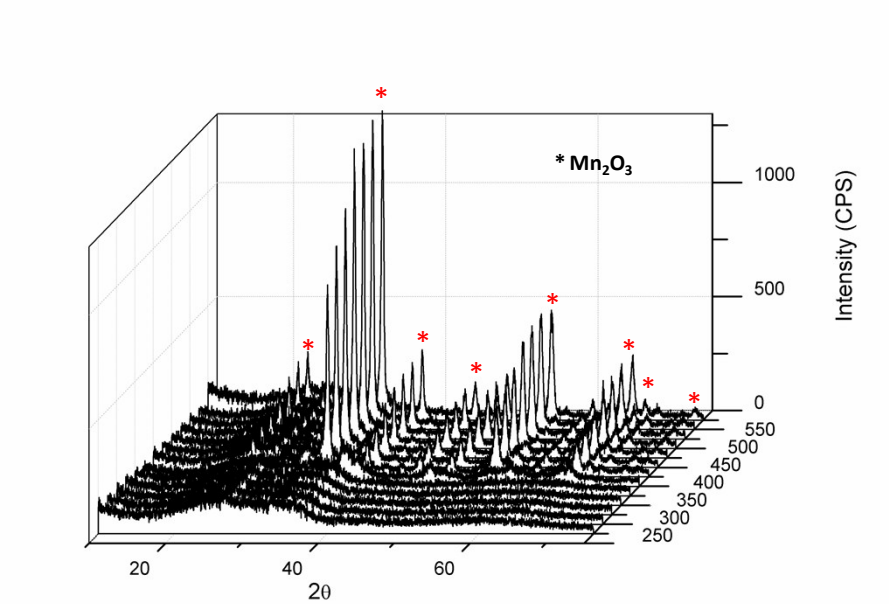

Fig. S12 The temperature resolved powder X-ray diffraction (TR-XRD) Cs-MnOx material under air. The material was calcined at 150°C for 12 h and 250°C for 3 h prior to measurement.

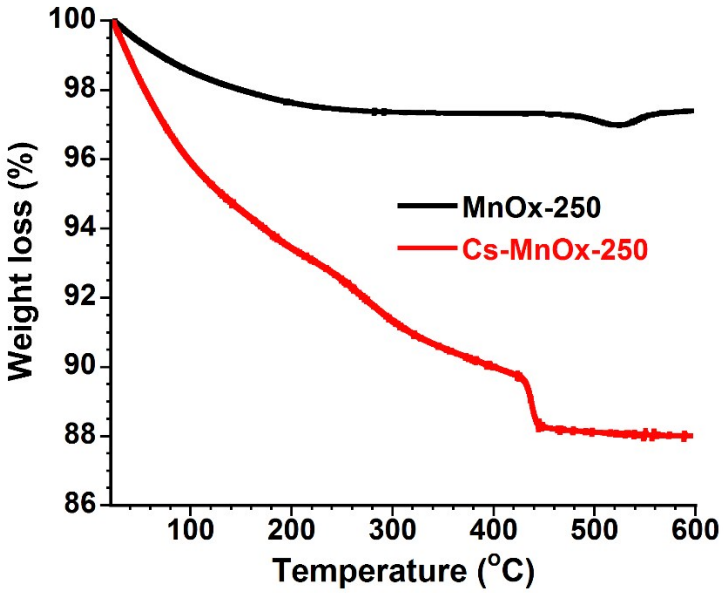

Fig. S13 The thermogravimetric analysis of Cs-MnOx and MnOx materials under air. Both of the materials were calcined at 150 °C for 12 h and 250 °C for 3 h prior to measurement.

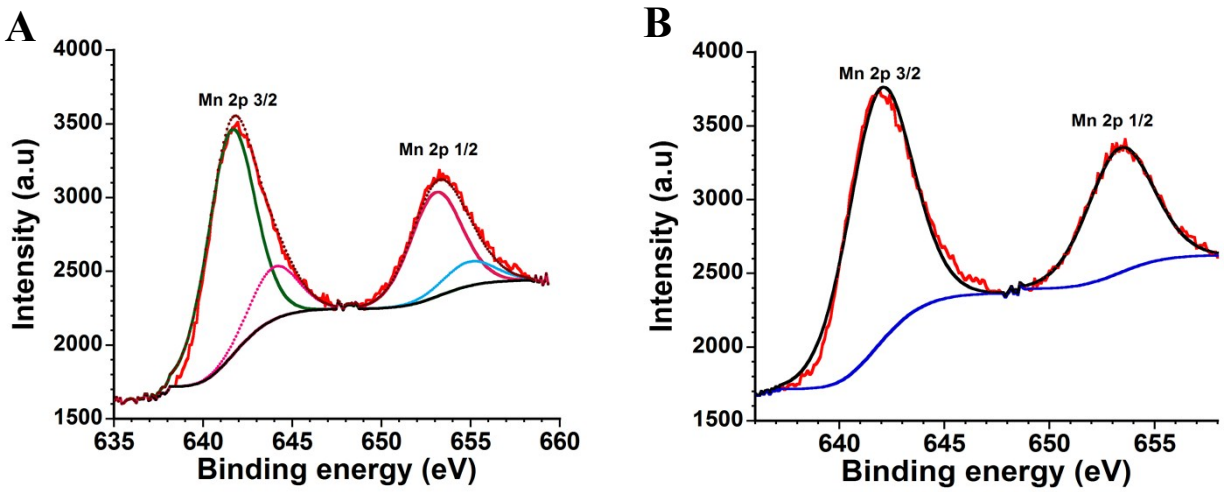

Fig. S14 XPS analysis of Mn 2p spectra of (A) MnOx-450 and (B) Cs-MnOx-450 materials. The MnOx material shows the presence of Mn^{3+} along with Mn^{4+} valency (Mn^{3+}/Mn^{4+}), whereas Cs-MnOx shows the presence of only Mn^{3+} species.

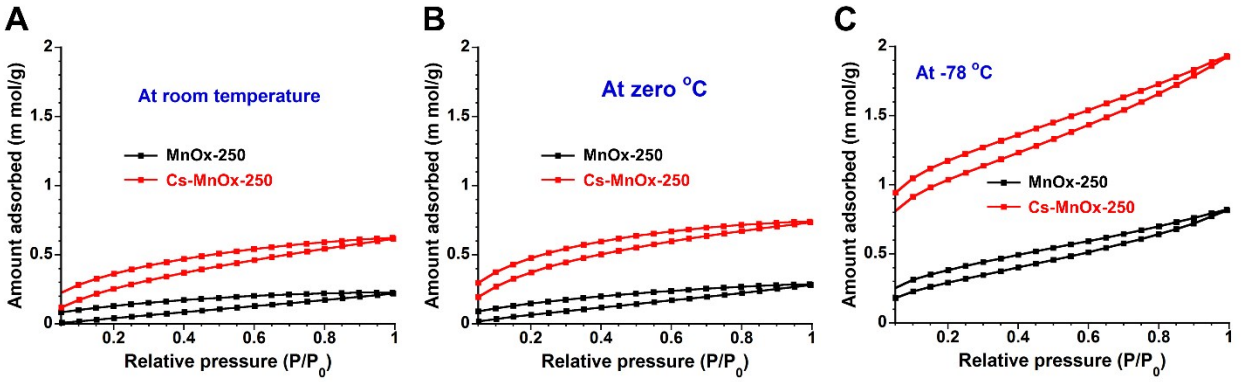

Fig. S15 The CO_2 adsorption of Cs-MnOx and MnOx materials calcined at 250 °C for 3 h at (A) RT, (B) 0 °C and, (C) -78 °C.

Density Functional Theory (DFT) study

Model Details and Methods

Model calculations were performed with density functional theory (DFT) as implemented in the VASP code. The semi-local (PBE) exchange-correlation approximation with a cutoff energy of 500 eV captured the valence O 2s, 2p and Mn 3p, 3d, 4s states. Electron-core interactions were treated by projector-augmented (PAW) potentials, and all calculations were spin polarized.

Surface stability for the 3 cases was measured by the surface energy:

$$\gamma = \frac{E_{surface} - n_{Mn}E_{bulk}^{MnOx} - (x * n_{Mn} - n_O)\mu_O}{2A}$$

$$\mu_O = \frac{1}{2}E_{O2}$$

Where, γ is the surface energy, $E_{surface}$ and E_{bulk}^{MnOx} are the total energy of the surface and bulk MnOx models, n_i is the number of atoms of element i, μ_O is the oxygen chemical potential and A is the total area of the slab. The factor of 2 in the denominator arises due to the symmetric nature of the slab created.

Using ORR mechanism mentioned in main text, the binding of the key adsorbates, namely, H* and OH* were studied on the three different surfaces, with their stabilities represented by binding energies (Table S4, Fig. S14).

$$E_{Bind} = \frac{E_{surface}^{adsorbate} - E_{surface}^{clean} - n_{ads}E_{adsorbate}}{n_{ads}} \quad (5)$$

where $E_{surface}^{adsorbate}$ and $E_{surface}^{clean}$ are the total energies of a surface with and without an adsorbate. $E_{adsorbate}$ is the energy of an individual adsorbate while, n_{ads} is the total number of adsorbate molecules on the surface. Irrespective of the surface termination, the OH* and H* adsorbates bind to the surfaces and give no indication of preferred dissociation surfaces. To further probe dissociation preference, we determined the ΔH_{rxn} (ΔH for reactions 2-4) for the 3 oxide surfaces (Table S5) using density functional theory (DFT) computations.

Table S4: Binding energy of OH and H on MnO_x terminated surfaces

Binding Species	**MnO [200]**	**Mn_2O_3 [222]**	**MnO_2 [110]**
OH	-2.59	-2.8	-2.27
H	-1.61	-2.64	-3.05

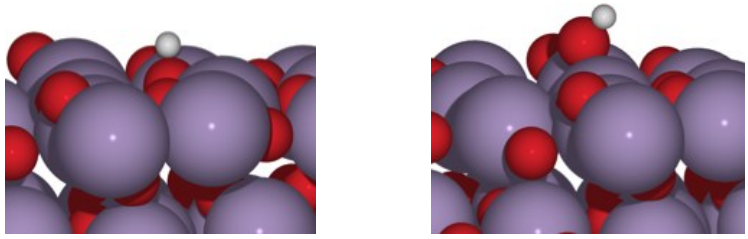

H* **OH***

Fig. S16. Model of H* and OH* adsorbate species on Mn_2O_3 surface

Table S5. Heat of Reaction for OER on the MnO_x terminated surfaces

Reaction	**MnO [200]**	**Mn_2O_3 [222]**	**MnO_2 [110]**
ΔH_1	3.94	2.91	2.5

ΔH_2	-2.49	-1.67	-0.73
ΔH_3	2.59	2.8	2.27

Table S6. Summary of the ORR activities of different manganese oxide electro-catalysts from the current study and the literature in alkaline medium (KOH).

Catalyst	E_j (V vs. RHE) @ -3 mA/cm^2 [a]	$E_{1/2}$ (V vs. RHE) [b]	Ref
Cs-MnOx-450	0.87	0.88	In this work
MnOx-450	0.64	0.79	In this work
Pt/C 20%	0.84	0.85	In this work
Manganese oxide Octahedral Molecular Sieve	0.82	0.81	1
MnOx nanowire on Ketjen black at 3200 rpm	~ 0.81	N/A	2
MnO-mesoporous nitrogen-doped carbon	0.79	0.81	3
$CaMn_3O_6$	0.77	0.78	4
H-MnO_2/C	N/A	0.77	5
α-MnO_2-SF	0.76	0.79	6
Ni-α-MnO_2-SF	0.75	0.81	6
α-MnO_2-HT	0.74	0.77	6

N-Graphene/MnO_x	0.73	N/A	7
Mn_2O_3 by atomic layer deposition	0.71	N/A	8
α-MnO_2 nanocrystal	0.7	0.73	9
Amorphous MnO_x	0.67	0.69	6
MnO_x-Graphene Oxide	0.6	N/A	10
β-MnO_2	0.52	0.71	6
δ-MnO_2	0.56	0.67	6
Thin film MnOx	0.73	N/A	11

[a] is the potential (V) vs. RHE measured at a current density of -3 mA/cm^2.
[b] is the half wave potential (V) vs. RHE.
All potentials were listed relative to the relative hydrogen electrode to facilitate the comparison. N/A stands for not applicable.

Table S7. Summary of the OER activities of different manganese oxide electro-catalysts from the current study and the literature compared to noble metal catalysts in alkaline medium.

Catalyst	E_j @ 10 mA/cm^2 [a]	Overpotential η (V) @ 10 mA/cm^2	Mass activity (A/g) [b] @ η = 0.45 V	TOF (s^{-1}) @ η = 0.45 V	ΔE (OER-ORR) (V)	Ref
Cs-MnOx-450	1.65	0.42	49	0.021	0.78	In this work
MnOx-450	1.72	0.49	7.8	0.003	1.08	In this work
Ir/C 20%	1.59	0.36	62	0.160	0.95	In this work
RuO_2	1.6	0.37	57	0.023	N/A	In this work
Pt/C 20%	2.01	0.78	< 1	N/A	1.17	In this work
α-MnO_2-HT	1.72	0.49	17.7	0.004	0.97	6
Ni-α-MnO_2-SF	1.74	0.51	23.4	0.003	1.00	6
MnO by ALD	1.84	0.61	N/A	N/A	N/A	8
Mn_2O_3 by ALD	1.81	0.57	N/A	N/A	1.1	8
Amorphous MnO_x	1.82	0.59	8.5	0.002	1.15	6
β-MnO_2	1.83	0.60	5.7	0.001	1.31	6
δ-MnO_2	1.97	0.74	4.2	0.001	1.41	6
$MnCo_2O_4$	> 1.65	> 0.42	N/A	N/A	N/A	12

[a] Potential (V) vs. RHE measured at a current density of 10 mA/cm^2. [b]Mass activity at $\eta = 0.45$ V, [c]Turn over frequency at $\eta = 0.45$ V((See experimental section for calculations of mass activity and TOF), [d]Potential difference between OER at 10 mA/cm^2 and ORR at -3 mA/cm^2.

References

1. A. M. El-Sawy, C. K. King'ondu, C.-H. Kuo, D. A. Kriz, C. J. Guild, Y. Meng, S. J. Frueh, S. Dharmarathna, S. N. Ehrlich and S. L. Suib, *Chem. Mater.*, 2014, **26**, 5752-5760.
2. J. S. Lee, G. S. Park, H. I. Lee, S. T. Kim, R. Cao, M. Liu and J. Cho, *Nano Lett.*, 2011, **11**, 5362-5366.
3. Y. Tan, C. Xu, G. Chen, X. Fang, N. Zheng and Q. Xie, *Adv. Funct. Mater.*, 2012, **22**, 4584-4591.
4. X. Han, T. Zhang, J. Du, F. Cheng and J. Chen, *Chem. Sci.*, 2013, **4**, 368-376.
5. T. Zhang, F. Cheng, J. Du, Y. Hu and J. Chen, *Adv. Ener. Mater.*, 2015, **5**, n/a-n/a.
6. Y. Meng, W. Song, H. Huang, Z. Ren, S. Y. Chen and S. L. Suib, *J. Am. Chem. Soc.*, 2014, **136**, 11452-11464.
7. T. Lee, E. K. Jeon and B.-S. Kim, *J. Mater. Chem. A*, 2014, **2**, 6167-6173.
8. K. L. Pickrahn, S. W. Park, Y. Gorlin, H.-B.-R. Lee, T. F. Jaramillo and S. F. Bent, *Adv. Ener. Mater.*, 2012, **2**, 1269-1277.
9. Y. Ma, R. Wang, H. Wang, J. Key and S. Ji, *J. Power Sources*, 2015, **280**, 526-532.
10. J. W. D. Ng, Y. Gorlin, D. Nordlund and T. F. Jaramillo, *J. Electrochem. Soc.*, 2014, **161**, D3105-D3112.
11. Y. Gorlin and T. F. Jaramillo, *J. Am. Chem. Soc.*, 2010, **132**, 13612-13614.
12. Y. Liang, H. Wang, J. Zhou, Y. Li, J. Wang, T. Regier and H. Dai, *J. Am. Chem. Soc.*, 2012, **134**, 3517-3523.